

# Chapter 6

## Determining Stress Intensity Factors Using Hybrid Thermoelastic Analysis

R.B. Vieira, G.L.G. Gonzáles, and J.L.F. Freire

**Abstract** This paper presents and discusses a technique suited for the determination of mode I Stress Intensity Factors (SIF) of fatigue-initiated and propagated cracks at the keyhole of polycarbonate specimens. A hybrid approach combined Thermoelastic Stress Analysis (TSA) results with Linear Elastic Fracture Mechanics solutions using Westergaard's stress function to describe the stress field near the crack tip. The TSA results used an experimental approach that does not require an infrared camera with lock-in capability. The experiments used a micro-bolometer camera A655sc from FLIR Inc. and a data processing software DeltaTherm2 from StressPhotonics Inc. Two distinct data fitting methods are presented. The first method measures the crack length, which makes the problem become linear, allowing for a simple Least Squares Method (LSM) approach. The second method, highlighting the true power of TSA as a fatigue analysis technique, uses the crack tip position as an adjustable parameter, making the problem non-linear and solvable by a complex numerical algorithm known as the Downhill Simplex Method (Nelder-Mead). The paper describes automated methodologies for making good initial estimates for the position of the crack, required by the non-linear approach, as well as for selecting data points to be fitted, both based on the loss of linearity of the TSA data due to non-adiabatic conditions.

**Keywords** Thermoelastic Stress Analysis • Micro-bolometer detector • Fatigue • Stress Intensity Factor • Polycarbonate

### 6.1 Introduction

Thermoelastic Stress Analysis (TSA) is a non-contact experimental technique that measures full-field stress maps for the surface of a component. It is based on the thermoelastic effect [1], which states that a cyclic loaded body experiences small temperature variations ( $\Delta T$ ), and that, if adiabatic conditions are satisfied, this variation is proportional to the first stress invariant.

Practical applications of TSA use infrared thermography to measure the very small pixel-by-pixel temperature variations. With these variations having been measured, Eq. (6.1) describes how the stress invariant is determined.

$$\Delta(\sigma_1 + \sigma_2) = A S \quad (6.1)$$

where  $\Delta\sigma_1$  and  $\Delta\sigma_2$  are the principal stress ranges acting on the observed point located at the surface,  $A$  is the thermoelastic calibration coefficient, and  $S$  is the magnitude of the TSA signal.

Combining the experimental data for the first stress invariant range, obtained through TSA, with an analytical solution for the crack tip stress-field, such as Westergaard stress function, the stress intensity factor (SIF) can be estimated.

Infrared detectors with enough sensitivity to measure such small temperature variations were very expensive in the past, but with recent advancements in micro-bolometer technology, the cost is going down quickly. The camera used to gather the experimental data presented in this paper is the A655sc from FLIR Inc., which has an uncooled micro-bolometric focal plane array detector and, as stated in [2], costs much, much less than the cooled quantum detectors that other authors have used.

DeltaTherm2, a new software program from Stress Photonics Inc., was used to convert the temperature data into TSA data. The typical TSA analysis involves a lock-in process, which correlates the  $\Delta T$  data with a reference signal, usually obtained from the function generator that feeds the cyclic actuator. DeltaTherm2 automates this process and takes the reference signal directly from the  $\Delta T$  measurements, making the whole TSA test much simpler to set up.

The SIF measurement algorithm was tested using numerically generated data that emulates the experimental TSA data for the stress field around a crack tip, and then was used to measure the SIF of a cracked SAE Keyhole specimen.

---

R.B. Vieira (✉) • G.L.G. Gonzáles • J.L.F. Freire

Pontifical Catholic University of Rio de Janeiro, Rua Marquês de São Vicente, 225, Gávea, Rio de Janeiro, RJ 22451-900, Brazil  
e-mail: [renato.bicharav@hotmail.com](mailto:renato.bicharav@hotmail.com)

Many authors have used TSA to measure SIFs, and they have also used varied numerical and experimental approaches. Stanley and Chan [3] used the first two terms of Westergaard's stress function to fit the thermoelastic data around cracks in mode I and II. Stanley and Dulieu-Smith [4] based their approach on the cardioid format of the isopachic fringes around a crack tip. Lesniak *et al.* [5] used Williams' stress field equations to fit the data using the least squares method (LSM). Lin *et al.* [6] approached the problem using the J-integral formulation in the data fitting process. Tomlinson *et al.* [7] developed a technique based on Muskhelishvili's stress field equations and a multipoint-over-deterministic method (MPODM). Díaz *et al.* [8] and [9] proposed a methodology for finding the crack tip position by looking at thermoelastic data, and then fitting the data using a non-linear approach in order to measure SIFs of propagating cracks. Marsavina *et al.* [10] used TSA to investigate crack closure during fatigue. Tomlinson and Olden [11] presented a broad review on the use of TSA in fracture mechanics and fatigue cracks.

The present work attempts to follow in these steps and develop an automated technique that can be used with an inexpensive infrared camera in combination with DeltaTherm2 software, which does not require a lock-in procedure.

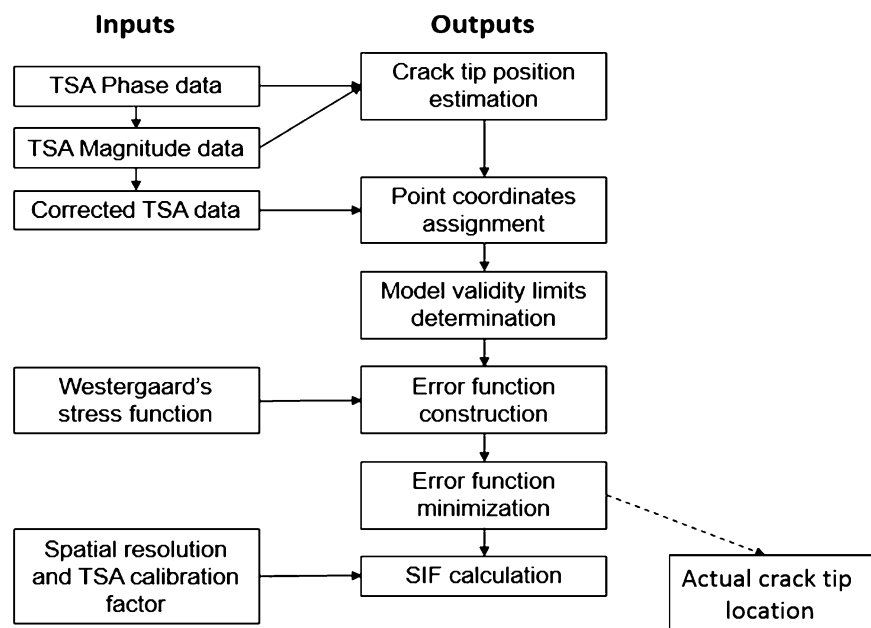
## 6.2 Description of the SIF Calculation Algorithm

Figure 6.1 shows a flowchart of the SIF calculation algorithm. The following sections describe each step.

## 6.3 Algorithm Inputs

The algorithm inputs are the outputs derived from the TSA analysis. The TSA data is usually expressed as a complex variable that has a magnitude and a phase angle. The magnitude is proportional to the temperature variation and thus, through Eq. (6.1), proportional to the variation of the first stress invariant. The phase angle carries the signal information, that is, if a stress should be treated as compressive or tensile.

**Fig. 6.1** Flowchart of the SIF calculation algorithm



In order to generate the phase data, the TSA software uses a reference signal and determines its phase difference from the temperature measurements. This is called the lock-in process. The most usual way to do this is to use an input from the cyclic loading machine as the reference; but as stated above, the software used in the present work does it differently. DeltaTherm2 uses the temperature of a selected area of the specimen's surface as the reference.

Subsequently, with the TSA magnitude and phase data, it is possible to generate corrected TSA data,

$$S = \begin{cases} Mag & \text{if } |phase| < 45^\circ \\ -Mag & \text{if } |phase| > 45^\circ \end{cases} \quad (6.2)$$

where S is the corrected TSA data, Mag is the magnitude data value in "camera units", and |phase| is the absolute value of the phase angle, in degrees.

Another input required is the mathematical model that is being used. In this case, a Westergaard's stress function (We) was used to describe the stress field around the crack tip [12]:

$$We(x, y) = \sigma_1 + \sigma_2 = 2[Re(Z) + Re(Y)] \quad (6.3)$$

with

$$\begin{aligned} Z &= \sum_{n=0}^N [A_n z^{n-0.5}] \\ Y &= \sum_{m=0}^M [B_m z^m] \end{aligned} \quad (6.4)$$

where N and M determine the number of coefficients to be used,  $A_n$  and  $B_m$  are the data fitting coefficients, and z is the complex variable of the point coordinates:

$$z = (x - x_o) + i(y - y_o) \quad (6.5)$$

Where x and y are the horizontal and vertical coordinates of a point (placing the origin at the estimated crack tip location), and  $i = \sqrt{-1}$  and  $x_o$  and  $y_o$  are the horizontal and vertical errors of the estimated crack tip location. These errors are solved only when applying the non-linear method; for the linear method they are set to 0.

The final required inputs are the spatial resolution (SR) and the TSA calibration factor (A). The spatial resolution is simply determined via a known dimension in the specimen,

$$SR = W/p \quad (6.6)$$

where SR is the spatial resolution in mm/pixel, W is a known dimension of the specimen in mm (i.e. width), and p is the number of pixels the dimension measures on the thermographic image.

There are many possible TSA calibration processes [13], but this work uses what may be the simplest one, which consists of using a specimen, machined from the same sheet of polycarbonate, with an analytically determined stress. Then, using Eq. (6.1) to correlate the calculated change of the stress invariant ( $\Delta\sigma_1 + \Delta\sigma_2$ ) and the measured TSA signal (S), A is determined for the camera-material pair.

## 6.4 Crack Tip Position Estimation and Point Coordinates Assignment

This work uses a specially improved, automated version of the methodology proposed in [8] to estimate the position of the crack tip.

First, the image needs to be positioned so that the crack is horizontal. Then, using the TSA magnitude map, the vertical position of the crack tip ( $Y_o'$ ) is estimated by plotting y vs.  $1/S^2$  curves for each vertical line in the image (perpendicular to the crack). The resulting graphs, for the lines ahead of the crack tip, have a clear minimum value. The mean value of y where this minimum value occurs for all the vertical lines is equal to  $Y_o'$ . Figure 6.2a shows the magnitude map around a crack, while Fig. 6.2b shows a typical y vs.  $1/S^2$  plot.

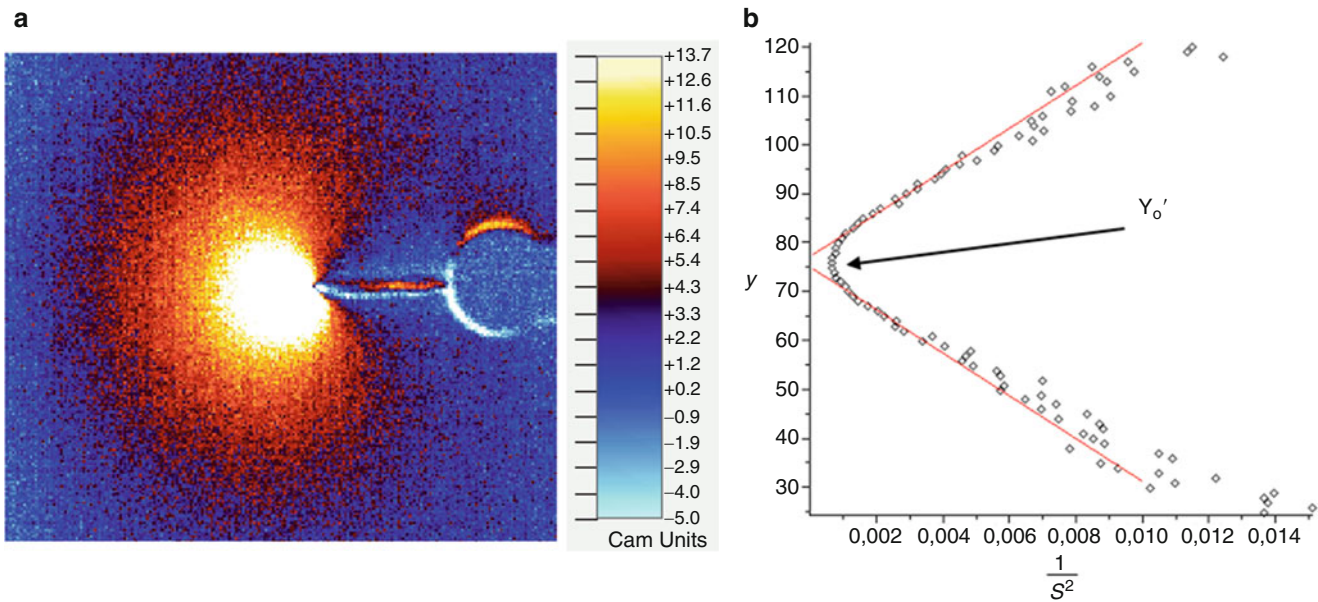


**Fig. 6.2** (a) Magnitude map around a crack and (b) Typical  $y$  vs.  $1/S^2$  plot

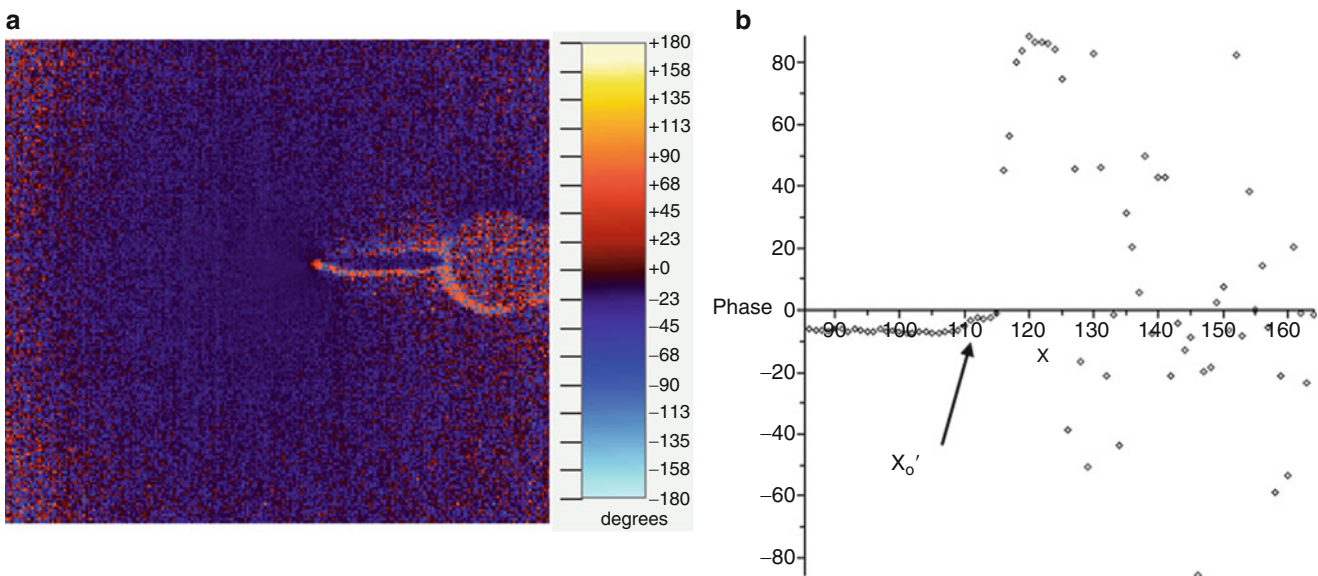
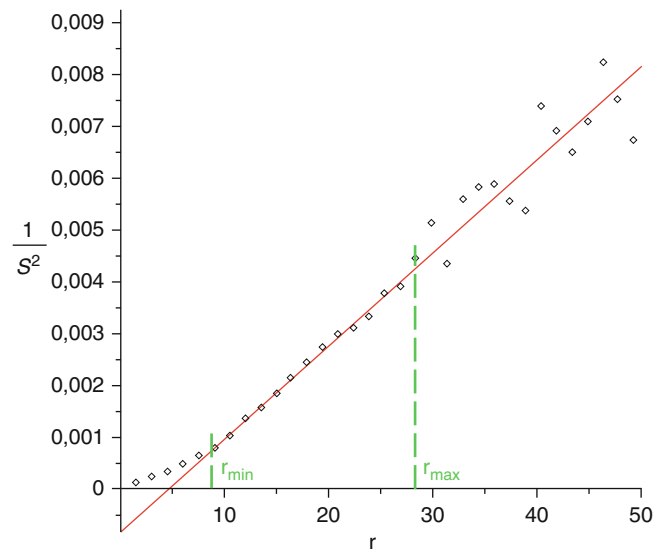


**Fig. 6.3** (a) Phase map around a crack and (b) Typical phase vs.  $x$  plot

The horizontal position of the crack tip ( $X_o'$ ) is estimated using what is called the phase shift. Due to the plasticity near the crack tip, the adiabatic conditions required by TSA are lost. This can be seen as an abrupt change in phase angle directly in front of the crack tip. In the horizontal phase vs.  $x$  curve at  $Y_o'$ , the position where this abrupt change occurs is equal to  $X_o'$ . Figure 6.3a shows the phase map around a crack and Fig. 6.3b shows a typical phase vs.  $x$  plot.

Having determined the values of  $X_o'$  and  $Y_o'$ , the coordinates assignment step is simple: each point of the image gets assigned to an  $x$  and a  $y$  value, which are the horizontal and vertical distances from the estimated crack tip, respectively.

**Fig. 6.4** Typical  $1/S^2$  vs.  $r$  plot



## 6.5 Model Validity Limits Verification

The points used for the data fitting process must be in accordance with the mathematical model. In [9], the authors concluded that the model predicts a linear behavior of  $1/S^2$  with respect to the distance from the crack tip. They proposed that only the points of Fig. 6.2b that presented a linear behavior should be used in the data fitting process.

The methodology used in the present work uses the same argument, but instead of using the vertical line plots, it uses plots of  $1/S^2$  vs.  $r$ , where  $r$  is the radial distance from the estimated crack tip. With  $r$  and  $\theta$  being the polar coordinates centered at  $X_o'$  and  $Y_o'$ , and  $\theta = 0$  being the horizontal line ahead of the crack,  $1/S^2$  vs.  $r$  curves are plotted for each  $1^\circ$  increment of  $\theta$  between  $-120^\circ$  and  $+120^\circ$ . Figure 6.4 shows an example of one of these plots.

The loss of linearity near the crack tip is explained by non-adiabatic conditions that interfere with the TSA results. For the region far away from the crack tip, there are two possible explanations, or a combination of both. The higher noise in TSA data due to smaller stresses and consequent smaller temperature variation, and the complexity of the actual stress field far from the crack, which requires not only the SIF term, but also more terms of the stress function to be predicted accurately.

For each of the  $1/S^2$  vs.  $r$  plots,  $r_{min}$ ,  $r_{max}$  values are determined using two margins of tolerance of non-linearity that are manually adjusted to fit the data. The authors assume that the  $r_{min}$  margin should be related to the loading level and that the  $r_{max}$  margin could be related to the overall noise levels of the data. No attempts were made to automate the optimization process of these margins.

The values  $R_{min}$  (and  $R_{max}$ ), below (and above) which no data points are collected, are defined as the mean value of all the  $r_{min}$  (and  $r_{max}$ ).

## 6.6 Error Function Construction and Minimization

After determining which data points can be fitted by the model, an error function ( $e$ ) is constructed:

$$e = \sum_{Data\ points} [S - We(x, y)]^2 \quad (6.7)$$

where  $e$  is the error function to be minimized,  $S$  is the TSA signal of the point, and  $We(x, y)$  is defined by Eq. (6.3).

For the linear approach, the minimization process uses an LSM algorithm and for the non-linear approach it uses a Downhill Simplex method (Nelder-Mead) [14].

## 6.7 SIF Calculation and Real Crack Tip Location

After having calculated all the coefficients, the SIF can be calculated as

$$\Delta K_I = A_0 A \sqrt{2\pi SR} \quad (6.8)$$

where  $\Delta K_I$  is the mode I SIF range in  $\text{MPa}\sqrt{\text{m}}$ ,  $A_0$  is the first coefficient as described in Eq. (6.4),  $A$  is the TSA calibration factor, and  $SR$  is the spatial resolution.

In the non-linear approach, the values of  $x_o$  and  $y_o$ , as seen in Eq. (6.5), are determined, as well as the real location of the crack tip:

$$\begin{aligned} X_o &= X'_o - x_o \\ Y_o &= Y'_o - y_o \end{aligned} \quad (6.9)$$

where  $X_o$  and  $Y_o$  give the calculated actual position of the crack tip.

## 6.8 Description of the Equipment

As stated above, the camera used in the experiments described below was the FLIR A655sc. It has a focal plane array detector composed of  $640 \times 480$  uncooled micro-bolometers and can record full-frame data at up to 50 Hz. It has a spatial resolution of  $17 \mu\text{m}$  and a sensitivity of 30 mK.

The camera is pointed at the specimen, which is mounted in a pneumatic machine capable of applying cyclic loads at a frequency of 5 Hz. A load cell (5000 N), connected in series with the specimen and the pneumatic muscle, sends the load signal to a computer program that controls the servo-valve. The load magnitude is controlled with a valve that regulates the air pressure entering the muscle. Figure 6.5 shows a photo of the system.

As stated previously, DeltaTherm2 does not require a reference signal from the load cell, so the camera and loading systems are completely separate.

**Fig. 6.5** Test system setup

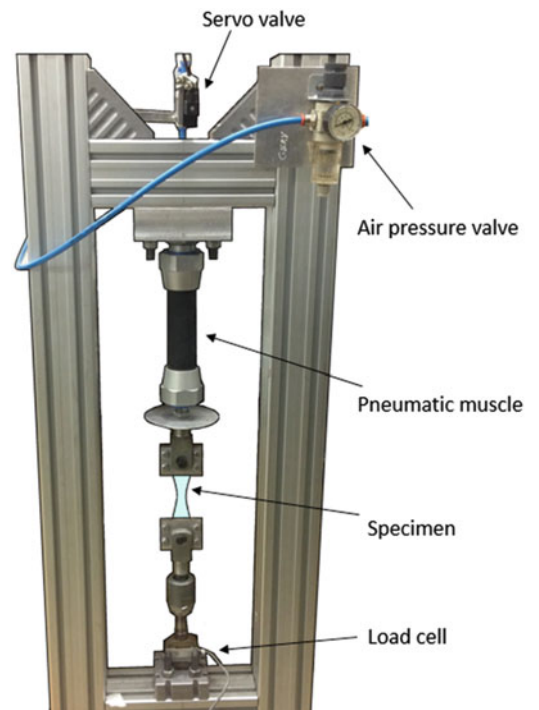
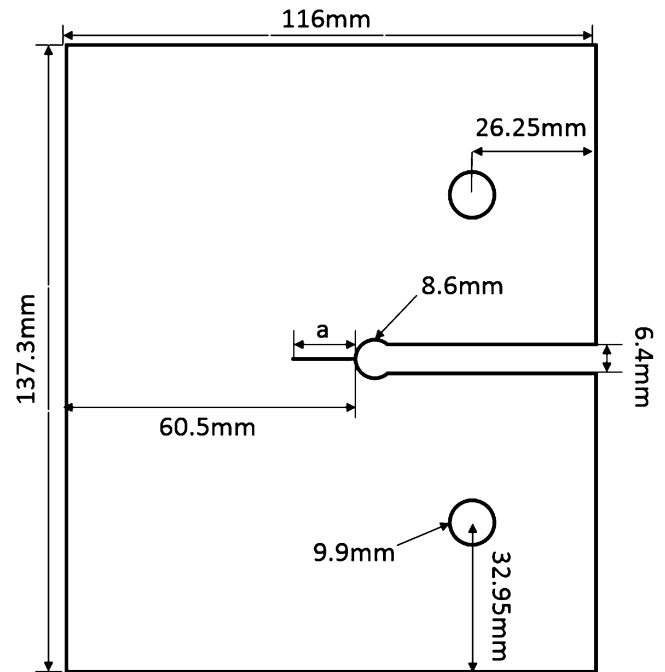


**Fig. 6.6** Keyhole specimen dimensions



## 6.9 Specimen

The specimen used in all the experiments was a SAE Keyhole specimen, which was developed to study both fatigue crack initiation and propagation. The dimensions of the specimen, machined from a 3.9 mm thick PALSUN<sup>TM</sup> polycarbonate (annealed) plate from PALRAM, are shown in Fig. 6.6.

## 6.10 Results

First, the algorithm is tested using an emulation of TSA data. Figure 6.7a shows the numerically generated data and Fig. 6.7b shows the fitted model for the crack tip estimation at  $(-3, 0)$  relative to the actual position.

For the linear approach, where the crack tip location is not determined, the result of  $\Delta K_I$  was heavily dependent on the crack tip horizontal position estimation ( $X_o'$ ), presenting errors of 10 % for just 1 pixel of inaccuracy in the estimation. For the vertical direction, the dependence was much smaller, a 1 pixel inaccuracy in  $Y_o'$  resulted in an error of 0.4 % for  $\Delta K_I$ .

The non-linear approach, on the other hand, gave on-point results for  $\Delta K_I$  even for initial crack-tip estimation coordinate ( $X_o'$  and  $Y_o'$ ) errors of 20+ pixels in the horizontal and vertical directions.

After having validated the methodology, the algorithm was put to the test on several crack lengths ( $a$ ) for the specimen shown in Figs. 6.2, 6.3 and 6.6. Table 6.1 shows the results for both the linear and non-linear approaches, as well as for Digital Image Correlation (DIC), as described in [15], and finite elements method (FEM) for the  $\Delta K_I$  [16]. Figure 6.8 shows the  $\Delta K_I/\Delta P$  vs.  $a$  plot.

The analyses were made using  $N = M = 3$ , as described in Eq. (6.4), and 800 data points uniformly spaced between  $R_{\min}$  and  $R_{\max}$  limiting circles.

It is clear that, for bigger cracks, where the stresses around the crack tip are higher and the experimental data is less noisy, both TSA Non-linear and DIC techniques result in values of  $\Delta K_I$  closer to the expected value, calculated by FEM. The TSA Linear approach tends to give higher results and increasing errors, probably because with longer cracks, the non-adiabatic zone becomes larger and the crack-tip position estimative error gets bigger.

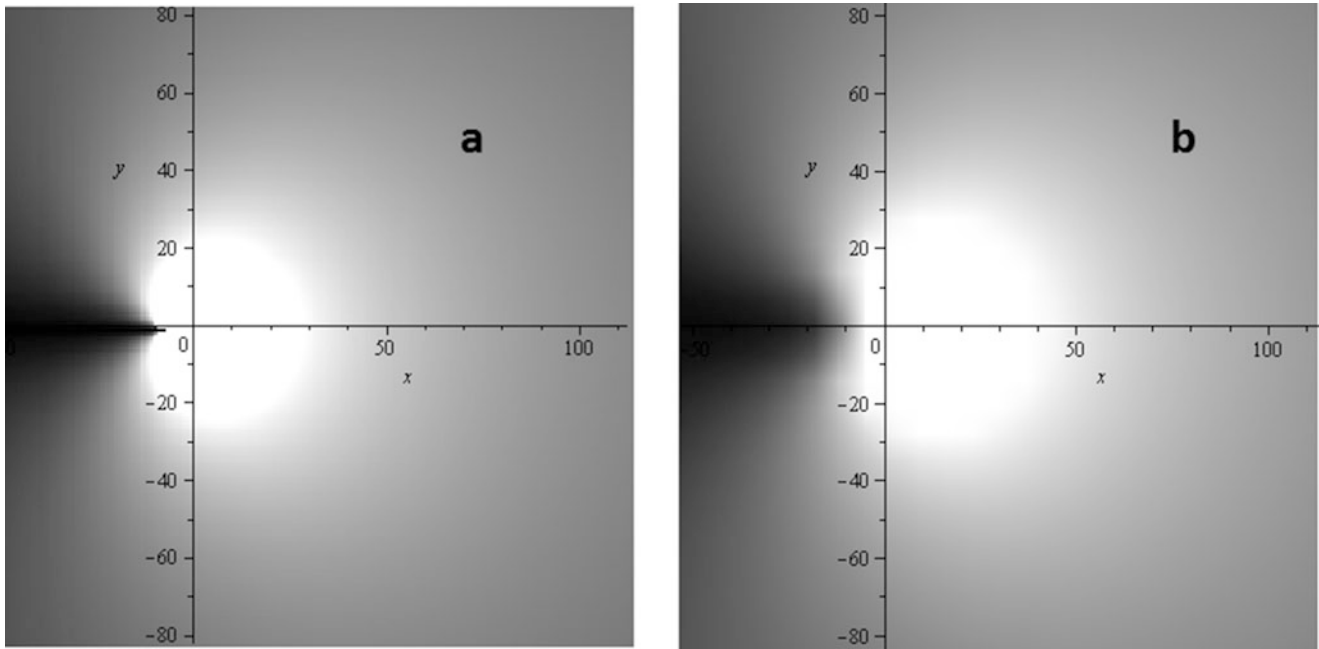
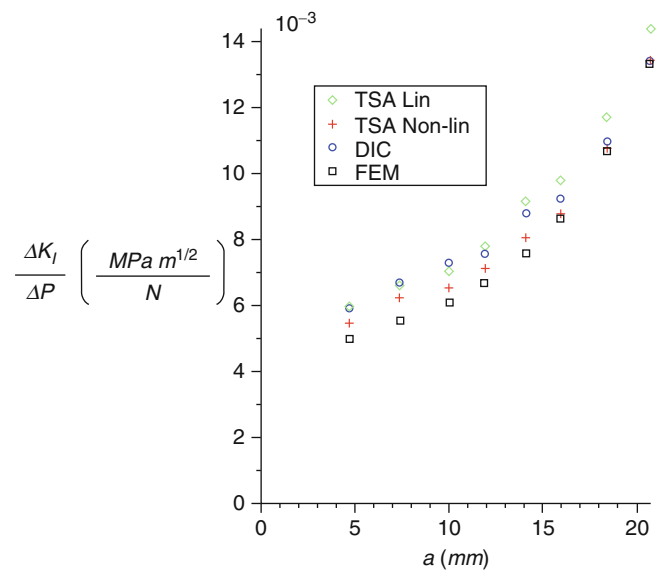


**Fig. 6.7** (a) Numerically generated TSA data and (b) Calculated model for a simulated crack tip located at  $(-3, -1)$  pixels

**Table 6.1** SIF Results for TSA (Linear and non-Linear), DIC and FEM

a (mm)	$\Delta P$ (N)	$\Delta K_I/\Delta P$ TSA Linear ( $10^{-3}$ MPa/N $\sqrt{m}$ )	$\Delta K_I/\Delta P$ TSA Non-linear ( $10^{-3}$ MPa/N $\sqrt{m}$ )	$\Delta K_I/\Delta P$ DIC ( $10^{-3}$ MPa/N $\sqrt{m}$ )	$\Delta K_I/\Delta P$ FEM ( $10^{-3}$ MPa/N $\sqrt{m}$ )
4.7	194	5.98	5.46	5.93	4.99
7.4	196	6.63	6.22	6.71	5.55
10	175	7.02	6.51	7.30	6.10
11.9	161	7.76	7.14	7.57	6.66
14.1	153	9.15	8.04	8.81	7.59
15.9	150	9.80	8.80	9.25	8.64
18.4	145	11.72	10.76	10.96	10.67
20.7	137	14.38	13.43	13.40	13.28

**Fig. 6.8**  $\Delta K_I/\Delta P$  vs. a plot for all experimental techniques and FEM





## 6.11 Conclusions

This work has outlined two methodologies—linear and non-linear—for determining SIF ranges using TSA with a relatively inexpensive, non-cooled micro-bolometric infrared camera coupled with a TSA software program that does not require a lock-in process. The results obtained for both are satisfactory when compared to DIC and FEM results.

The non-linear approach has some clear advantages and presents consistently better results than the linear solution, using FEA as the reference value. The main advantage of the linear approach is simplicity, which makes it faster to run, although no effort was made in the direction of optimizing the algorithms for run speed.

The process of SIF calculation using TSA was automated. The only manual input required at the current stage is the margins of tolerance for non-linearity verification in the model validity limits determination process. If the optimization of these margins were automatic, the algorithm could potentially be used to measure SIF ranges in real-time during crack propagation, although some run-speed improvements would be necessary.

## References

1. Dulieu-Barton, J.M.: Introduction to thermoelastic stress analysis. *Strain* **35**(2), 35–39 (1999)
2. Rajik, N., Rowlands, D.: Thermoelastic stress analysis with a compact low-cost microbolometer system. *Quant. Infrared Thermogr. J.* **10**(2), 135–158 (2013)
3. Stanley, P., Chan, W.K.: The determination of stress intensity factors and crack tip velocities from thermoelastic infra-red emissions. In: *Proceedings of International Conference of Fatigue of Engineering Materials and Structures*, c262, IMechE, Sheffield, UK, pp. 105–114 (1986)
4. Stanley, P., Dulieu-Smith, J.M.: Progress in the thermoelastic evaluation of mixed mode stress intensity factors. In: *Proceedings of the SEM Spring Conference on Experimental Mechanics*, Dearborn, pp. 617–626 (1993)
5. Lesniak, J.R., Bazile, D.J., Boyce, B.R., Zickel, M.J., Cramer, K.E., Welch, C.S.: Stress intensity measurement via infrared focal plane array. *Non-Traditional Methods of Sensing Stress, Strain, and Damage in Materials and Structures*. ASTM STP 1318, Philadelphia (1997)
6. Lin, S.T., Feng, Z., Rowlands, R.E.: Thermoelastic determination of stress intensity factors in orthotropic composites using the J-integral. *Eng. Fract. Mech.* **56**, 579–592 (1997)
7. Tomlinson, R.A., Nurse, A.D., Patterson, E.A.: On determining stress intensity factors for mixed mode cracks from thermoelastic data. *Fatigue Fract. Eng. Mater. Struct.* **20**, 217–226 (1997)
8. Díaz, F.A., Yates, J.R., Tomlinson, R.A., Patterson, E.A.: Some observation on the application of thermoelasticity to fatigue cracks. In: *Proceedings of SEM Conference*, Milwaukee, USA (2002)
9. Díaz, F.A., Patterson, E.A., Tomlinson, R.A., Yates, J.R.: Measuring stress intensity factors during fatigue crack growth using thermoelasticity. *Fatigue Fract. Eng. Mater. Struct.* **27**, 571–583 (2004)
10. Marsavina, L., Tomlinson, R.A., Patterson, E.A., Yates, J.R.: Investigation of crack closure by using thermoelastic stress analysis. In: *Proceedings of the 16th European Conference of Fracture*, Alexandroupoulos, Greece (2006)
11. Tomlinson, R.A., Olden, E.J.: Thermoelasticity for the analysis of crack tip stress fields—a review. *Strain* **35**(2), 49–55 (1999)
12. Shukla, A., Dally, J.W.: *Experimental Solid Mechanics*. College Enterprises (2010)
13. Dulieu-Smith, J.M.: Alternative calibration techniques for quantitative thermoelastic stress analysis. *Strain* **31**, 9–16 (1995)
14. Nelder, J.A., Mead, R.: A simplex method for function minimization. *Comput. J.* **7**, 308–313 (1965)
15. Gonzáles, G.L.G., Díaz, J.G., Gonzáles, J.A.O., Castro, J.T.P., Freire, J.L.F.: Approaches for determining stress intensity factors of fatigue propagating cracks using DIC. In: *Proceedings of the SEM Annual Conference on Experimental Mechanics*, Orlando, 6–9 June 2016
16. Vieira, R.B.: Thermography applied to the study of fatigue in polycarbonate. MSc thesis, Departamento de Engenharia Mecânica, Pontifícia Universidade Católica do Rio de Janeiro, PUC-Rio, (2016)